Journal of Luminescence 230 (2021) 117749

Contents lists available at ScienceDirect

Journal of Luminescence

journal homepage: http://www.elsevier.com/locate/jlumin

Full Length Article

Phase transition, radio- and photoluminescence of $K_3Lu(PO_4)_2$ doped with Pr^{3+} ions

Konstantin V. Ivanovskikh [a,*], Vladimir A. Pustovarov [a], Sergey Omelkov [b], Marco Kirm [b], Fabio Piccinelli [c], Marco Bettinelli [c]

[a] Institute of Physics and Technology, Ural Federal University, 19 Mira St., 620002, Ekaterinburg, Russia
[b] Institute of Physics, University of Tartu, 1 W. Ostwald St., 50411, Tartu, Estonia
[c] Laboratory of Luminescent Materials, Department of Biotechnology, University of Verona and INSTM, UdR Verona, Strada Le Grazie 15, I-37134, Verona, Italy

ARTICLE INFO

Keywords:
$K_3Lu(PO_4)_2$
Pr^{3+} $4f^15d \rightarrow 4f^2$ transitions
Defects
Host-to-impurity energy transfer
Radioluminescence
Phase transitions
PACS: 78.55.-m
78.47.D

ABSTRACT

Luminescent characteristics of $K_3Lu(PO_4)_2$:Pr^{3+} (1 and 5 mol.%) microcrystalline powders, a promising optical material for scintillation applications, were investigated using various experimental techniques. The material shows emission features connected with both high intensity interconfigurational $4f^15d \rightarrow 4f^2$ transitions (broad UV emission bands) and intraconfigurational $4f^2 \rightarrow 4f^2$ transitions (weak emission lines in the visible range). The output of X-ray excited $4f^15d \rightarrow 4f^2$ emission of Pr^{3+} increases with a temperature rise from 90 K to room temperature and higher depending on the Pr^{3+} ions concentration. The high 5% concentration of Pr^{3+} ions is found to be favourable for the stabilization of a monoclinic phase ($P2_1/m$ space group) over a trigonal one ($P\bar{3}$ space group) while emission properties of the material reveal that a phase transition occurs at higher temperatures. Decay kinetics of Pr^{3+} $4f^15d \rightarrow 4f^2$ emission are recorded upon excitation with high repetition rate X-ray synchrotron excitation and pulse cathode ray excitation. Issues related to a non-exponential decay of luminescence and presence of slow decay components are discussed in terms of energy transfer dynamics. The presence of defects was revealed with thermoluminescence measurements and these are suggested to be the mainly responsible for delayed recombination of charge carriers on the Pr^{3+} $4f^15d$ states. Some peculiarities of host-to-impurity energy transfer are discussed.

1. Introduction

Scintillator materials remain main media for detection of ionising radiation and are widely applied in dosimetry, nuclear physics, medical imaging, environmental studies, geological exploration, security, chemistry, space physics, etc. Some highly demanding applications such as nuclear physics or medical imaging (e.g. time-of-flight PET scanners) require scintillators with prominent properties in terms of timing, light output, material density and Z_{eff}. As long as all the desirable properties are hard to achieve with a single particular material, studies in this field are still active and aimed in search of scintillator materials capable to meet most critical requirements in particular field of an application. Among fast scintillator materials promising for medical imaging technologies research efforts have mostly been expanded on inorganic oxides, particularly silicates, garnets, phosphates, and binary rare earth halides doped with Ce^{3+} or Pr^{3+} ions which demonstrate fast emission due to their interconfigurational 5 d-4f transitions [1–14].

Among the new materials, $K_3Lu(PO_4)_2$ (KLuP) doped with Pr^{3+} ions was identified as promising compound for scintillator applications. The material has density of 3.9 g/cm^3 at room temperature (RT) and Z_{eff} of about 44.5. A time-resolved and temperature-dependent luminescence study under vacuum ultraviolet (VUV) excitation revealed that the $K_3Lu(PO_4)_2$ is able to efficiently transfer energy of host electronic excitations to Pr^{3+} dopant ions either in case of the low-temperature monoclinic or high-temperature trigonal phase of material [12]. The next step in study of Pr^{3+}-doped KLuP was recently realized in Refs. [14], where understanding on phase-dependent luminescence properties of Pr-doped $K_3Lu_{1-x}Y_x(PO_4)_2$ solid solutions was demonstrated. The authors showed that the monoclinic phase can be obtained when Y/Lu ratio in the solid solution is above 0.16. It was also revealed that the ratio of Pr^{3+} $4f^15$ d-$4f^2$ and $4f^2$-$4f^2$ emission intensities ratio progressively decreases when Y concentration is increased. To promote application of KLuP:Pr^{3+} as a scintillator further studies towards understanding of temperature dependence of its luminescence properties upon excitation with

* Corresponding author.
E-mail address: k.v.ivanovskikh@urfu.ru (K.V. Ivanovskikh).

https://doi.org/10.1016/j.jlumin.2020.117749
Received 4 August 2020; Received in revised form 29 October 2020; Accepted 2 November 2020
Available online 5 November 2020

ionising radiation are required.

In this paper, we focused on the study of luminescence spectra (including time-resolved ones) and decay kinetics of moderately (1%) and highly (5%) doped KLuP upon X- and cathode ray excitation in wide temperature range. In addition, temperature dependences of X-ray excited luminescence yield and thermally stimulated luminescence (TL) glow curves were studied. The underlying idea for this research was that a high concentration (5%) of Pr^{3+} ions increases the stability of the monoclinic phase, that makes phase transitions to occur at higher temperatures. As a result, one can expect enhancement of KLuP: Pr^{3+} radioluminescence and its thermal stability will be improved. However, this effect has its limitation due to concentration quenching.

2. Synthesis and crystal structure characterisation

Polycrystalline samples of $K_3Lu(PO_4)_2$ doped with 1 and 5 mol% of Pr^{3+} (substituting for Lu^{3+}) were synthesized using a solid state reaction and verified for phase purity using X-ray diffraction (XRD) at the Laboratory of Luminescent Materials, University of Verona (Italy). The constituent raw powder materials of K_2CO_3 (99%), $(NH_4)_2HPO_4$ (>99%), Lu_2O_3 (Aldrich, 99.99%), and Pr_6O_{11} (Aldrich, 99.999%) were mixed and pressed into pellets under a load of 10 tons. The samples underwent two thermal treatments under air atmosphere (600 °C for 4 h and 950 °C for 1 h), with intermediate grindings and subsequent final grinding into white powder. Crystal structure of the samples was then examined using powder X-ray diffraction (PXRD) technique with a Shimadzu XRD-7000 X-ray diffractometer (see Fig. 1).

The XRD studies previously performed by some of us in Refs. [12] have established that the Pr^{3+}-doped $K_3Lu(PO_4)_2$ undergoes various structural phase transitions. At RT $K_3Lu(PO_4)_2$ crystallizes with a trigonal unit cell, $P\bar{3}$ space group. In this case, the Lutetium ion is six-coordinated by surrounding oxygen atoms of the phosphate groups with two non-equivalent sites in the crystal lattice. $K_3Lu(PO_4)_2$ host material has two phase transitions that occur at lower temperature. The first transition takes place near 250 K that results in a monoclinic phase ($P2_1/m$ space group), where Lu^{3+} ion retains the six-fold coordination. The second phase transition occurring near 140 K leads to a crystal structure with the same monoclinic space group while coordination of Lu^{3+} ion changes to a 7-fold one [11, 12].

Fig. 1 shows simulated XRD patterns compared with the corresponding experimental ones. The diffraction intensities of the simulated patterns were not corrected for preferential orientation. All the diffraction peaks in the XRPD pattern of the 1% Pr^{3+} doped KLuP sample are compatible with the ICDD data of the trigonal ($P\bar{3}$ space group) KLuP (PDF Card # 01-085-1586). No other phases were detected indicating that the sample synthesized is a single phase at RT. Detailed XRD analysis data and differential scanning calorimetry experiments data in 1% Pr^{3+}-doped KLuP were presented previously [12]. The samples doped with 5% Pr^{3+} show some extra peaks in the XRD pattern (Fig. 1, red pattern) which is compatible with the presence of a single monoclinic phase ($P2_1/m$ space group) already reported in the literature [ICSD card number 191225, Ref. [15] In both samples, the presence of preferential orientation of some crystallites gives rise to an abnormal high intensity of the peaks around 10° and 47° of 2θ (indexes reported in bold blue and red in Fig. 1). The peaks in the $P\bar{3}$ space group belong to the (00l) family, whilst those in the $P2_1/m$ space group belong to the (h00) one (Fig. 1).

3. Experimental details

Experimental results of this paper were obtained applying different techniques. Emission and photoluminescence (PL) excitation spectra upon excitation in the UV energy range (from 3.5 to 5.8 eV) were studied at the Laboratory of Solid State Physics, Ural Federal University. To excite the luminescence a 400 W deuterium lamp and a LOMO DMR-4

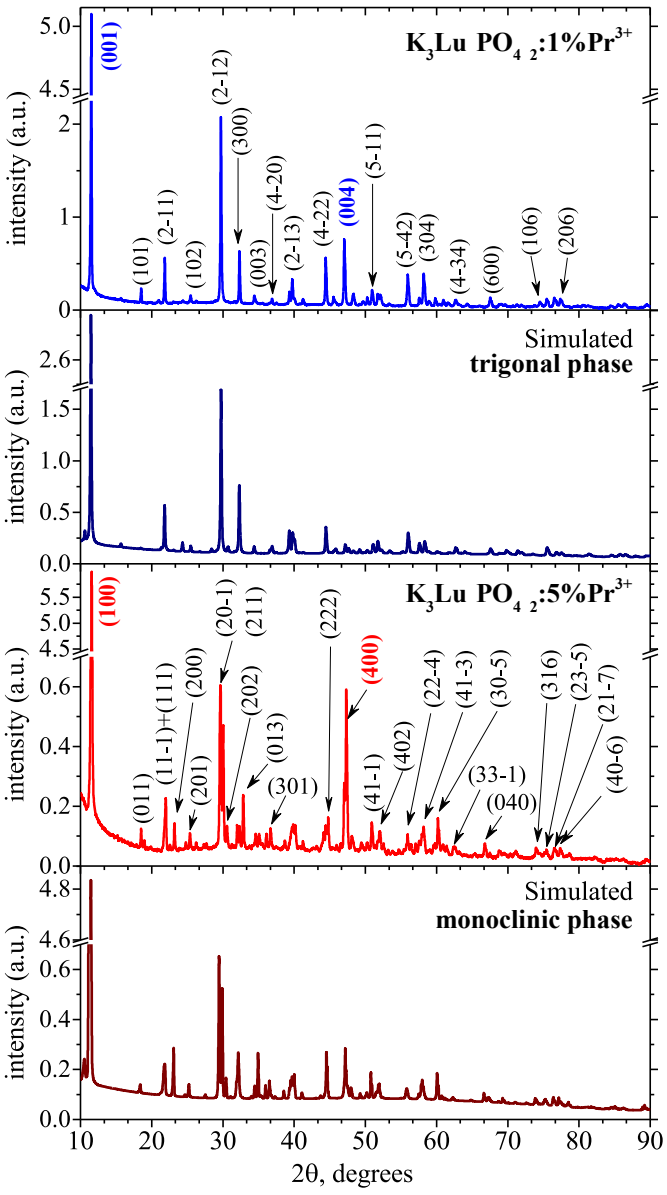

Fig. 1. Experimental and simulated PXRD patterns of KLuP:1%Pr^{3+} and KLuP:5%Pr^{3+} powdered samples at RT. The main peaks are indexed according to the reference cards (ICSD cards # 191224 and # 191225 for trigonal and monoclinic KLuP, respectively).

primary double prism monochromator were used. A secondary DMR-4 prismatic monochromator equipped with a Hamamatsu R6358-10 photomultiplier (PMT) was used to detect the luminescence signal. The X-ray excited studies performed at the same laboratory included measurements of X-ray excited luminescence (XRL) spectra and thermally stimulated luminescence (TSL) glow curves. The luminescence was analysed using a LOMO MDR-23 monochromator equipped with a FEU-106 PMT detector. A BSV-2 X-ray source (30 kV, 10 mA, Cu anode) was used for excitation. TSL glow curves were measured within the temperature range of 90–610 K after X-ray irradiation at T = 90 or 295 K with a heating rate of 0.33 K/s.

The measurements of decay kinetics and emission spectra upon excitation with poly-monochromatic "white beam" X-ray synchrotron radiation (E = 3–60 keV, pulse FWHM = 1 ns, repetition rate ~ 8 MHz) were performed at the beamline #6 of the VEPP-3 storage ring at the Budker Institute of Nuclear Physics (Russia). To detect the XRL a stroboscopic method of electron-optical chronography with sub-nanosecond

time resolution was used. The detection system included a SOL Instruments MS2004 monochromator equipped with a high-speed LI-602 dissector [16].

The pulsed cathodoluminescence (PCL) spectra and PCL decay kinetics were recorded upon excitation with a Radan-303 A pulse electron gun (E_{max} = 120 keV, pulse FWHM = 200 ps, rate 5 Hz) at University of Tartu (Estonia). An Andor Shamrock 303i monochromator equipped with either a Hamamatsu R3809U-50 MCP-PMT detector or cooled Andor iStar iCCD-camera was used for the registration [17].

All the emission spectra were corrected for the spectral sensitivity of the detection systems. PL excitation spectra were corrected for the wavelength-dependent photon flux variation using Lumogen F Yellow dye.

4. Results and discussion

4.1. X-ray and cathode-ray excited luminescence spectra

Fig. 2 demonstrates steady-stay XRL spectra of 1% Pr^{3+} and 5% Pr^{3+}-doped KLuP recorded at T = 90, 295 and 570 K. The XRL spectra obtained at T = 90 K where KLuP possesses the monoclinic structure are almost identical in case of 1% Pr^{3+} and 5% Pr^{3+} doping. Particularly the spectra are dominated broad UV emission bands assigned to interconfigurational transitions from the lowest Pr^{3+} $4f^15d^1$ state to the ^3H_J and ^3F_J multiplets of the ground $4f^2$ electronic configuration ($4f^15d^1 \rightarrow 4f^2$ transitions). The narrow emission features in the visible range near 483 and 605 nm are attributed to $4f^2 \rightarrow 4f^2$ intraconfigurational transitions, namely $^3P_0 \rightarrow {}^3H_4$ and $^1D_2 \rightarrow {}^3H_4$, respectively (see the assignments in Fig. 2).

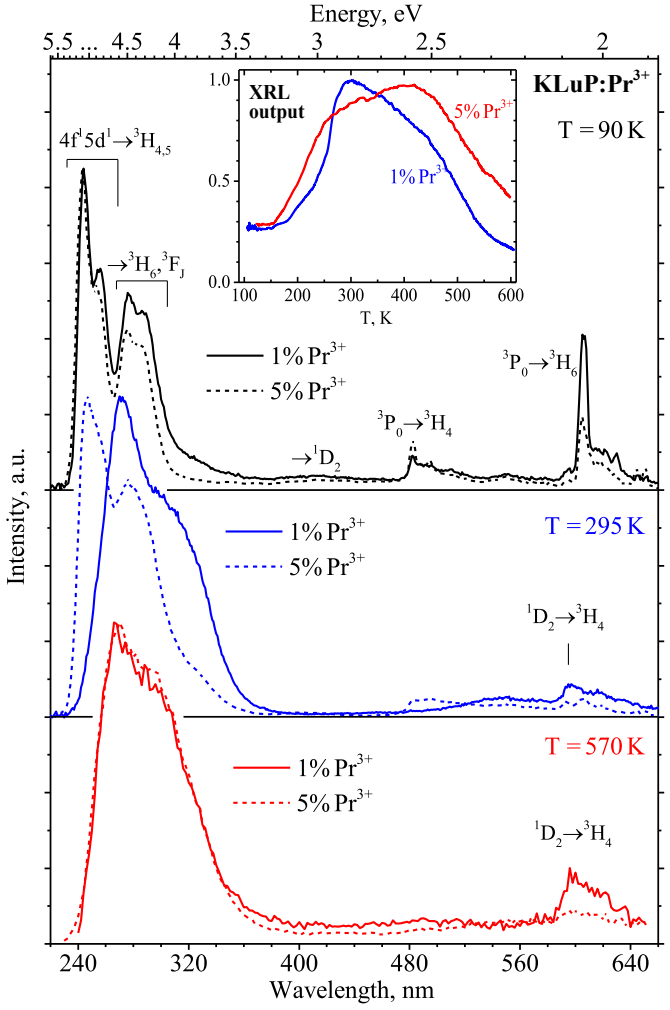

Fig. 2. Normalized XRL spectra of 1% Pr^{3+} and 5% Pr^{3+} doped KLuP samples at 90, 295 and 570 K. Inset shows temperature dependences of $4f^15d \rightarrow 4f^2$ XRL recorded for 1% Pr^{3+} and 5% Pr^{3+} doped KLuP samples as monitored at 270 nm and 278 nm, respectively.

The XRL spectra of KLuP doped with 1% Pr^{3+} and 5% Pr^{3+} recorded at RT, typical for trigonal phase of the KLuP crystal lattice according to Ref. [12, 14], reveal a noticeable difference between those, consisting in appearance of the $4f^15d^1 \rightarrow 4f^2$ emission band in the UV range. In the case of highly-doped sample this band appears just slightly less resolved while the barycentres of sub-bands representing transitions terminating at $^3H_{4,5}$ (near 246 nm) and $^3H_6$, ^3F_J multiplets (near 280 nm) keep located at the same spectral positions. In contrast, in the case of 1% Pr^{3+}-doped sample the $4f^15d^1 \rightarrow 4f^2$ emission band appears to be red-shifted for about 0.47 eV while shape of the band still has distinguishable sub-bands related to the transitions terminating at $^3H_{4,5}$ (near 271 nm) and $^3H_6$,^3F_J multiplets (near 315 nm) (see Fig. 2). Moreover, the $4f^15d^1 \rightarrow 4f^2$ emission band of 1% Pr^{3+} -sample demonstrates broadening relative to that of 5% Pr^{3+}-doped sample that indicates the presence of emission centers of two types at RT. The latter is consistent with availability of two distinct crystallographic sites for Pr^{3+} in the RT trigonal KLuP phase. We note that in general the XRL spectrum of 1% Pr^{3+}-doped sample presented here is in good agreement with that recorded upon intracentre excitation at λ_{ex} = 190 nm and reported earlier in Ref. [12]. The observed shift of the $4f^15d^1 \rightarrow 4f^2$ emission band reflects switching of the KLuP crystal structure to trigonal phase and corresponding changes of symmetry and local coordination at lutetium sites (substituted by Pr^{3+} ions). The $4f^15d^1 \rightarrow 4f^2$ emissions of XRL spectra for 1% Pr^{3+} and 5% Pr^{3+} doped KLuP samples overlap with each other at T = 570 K (Fig. 2) forming a wide structureless bands. These observations indicate that higher Pr^{3+} doping concentration is favourable for shifting the monoclinic-to-trigonal phase transition temperature well above RT.

Tuning of crystal structure and symmetry was well demonstrated for potassium rare-earth double phosphates on example of $K_3Lu_{1-x}Y_x(PO_4)_2$ solid solution in Ref. [14]. The authors showed that the crystal structure of the solid solution turns from trigonal to monoclinic phase while increasing Y^{3+} content from 0 to 1 relative to Lu^{3+}. Since in KLuP the dopand Pr^{3+} ions (ionic radius 0.99 Å, in six-fold coordination) substitute only for the Lu^{3+} ions (ionic radius 0.86 Å, in six-fold coordination [18]), the changes observed in the emission spectra when the system undergoes the phase transition, have to be linked to the crystal structure transformation and, consequently, to the local Pr^{3+} coordination and symmetry changes.

Based on the XRD analysis performed in Ref. [12] it is assumed that energy of the Pr^{3+} 5*d*-4*f* emission band in 1% Pr^{3+}-doped KLuP strongly depends on both the covalence effect and the crystal field strength induced by the ligands. As a result of covalent bonding between the 5*d* and the ligand orbitals, the 5*d* orbitals expand and become partially delocalized over the ligands, that in turn lowers the energy of the 5*d* states. The red shift of the 5*d*-4*f* emission band observed when temperature increases from 8 to 300 K is linked to a possible increase of the covalency of the Pr–O bonds that results in an increase of the monoclinic to trigonal phase transition temperature.

We note that this effect is also well demonstrated by temperature dependences of $4f^15d \rightarrow 4f^2$ XRL quantum yield recorded for 1% Pr^{3+} and 5% Pr^{3+} doped samples as monitored at 270 and 278 nm, respectively (see Inset in Fig. 2). The XRL intensity gradually rises when temperature increases from 90 to 300–400 K for the both samples. Such a temperature dependence observed for a luminescence excited through recombinational energy transfer [12] implies the occurrence of alternative (competing) paths for feeding the impurity excited states through capture of thermally liberated charge carriers from shallow traps. The presence of shallow traps in the samples is demonstrated below by thermally stimulated luminescence measurements (see Section 4.3). Moreover, we do not exclude that the presence of phase transitions at T = 140 K and T = 250 K may also influence the XRL temperature

dependences. The temperature dependences of $4f^15d^1 \rightarrow 4f^2$ XRL intensity demonstrate maximum near 300 K and 410 K for 1% Pr^{3+} and 5% Pr^{3+} KLuP, respectively. Further increase of temperature leads to the gradual decrease of XRL quantum yield while quenching temperature T_Q, that is defined as the temperature at which the XRL output drops to 50% of its maximum value, is $T_{Q1} = 495$ K and $T_{Q5} = 570$ K for 1% and 5% Pr^{3+} -doped KLuP, respectively. The thermal quenching mechanism in KLuP:Pr^{3+} can be connected with either non-radiative relaxation from the 5*d* state to the 4*f* state described by a configurational coordinate diagram or a thermally induced photoionization. The former one is determined by a Stokes shift for $4f^15d^1 \leftrightarrow 4f^2$ transition that will be estimated below in Section 4.3. The latter one is obviously related to a thermally induced ionization of 5*d* state, depending on its energetic position relative to the bottom of conduction band that can be further prompted by the presence of shallow traps. A multiphonon relaxation of the lowest 5*d* state can be excluded as no enhancement of $4f^2 \leftrightarrow 4f^2$ is observed with the temperature increasing.

Fig. 3 shows time-resolved PCL spectra measured at T = 295 K. The spectra were taken within two independent time gates (TG) which collect the emission signal within 32 ns ('fast' TG) and 2 ms ('slow' TG) after the excitation cathode ray pulse. As expected, the $4f^15d^1 \rightarrow 4f^2$ emission band solely dominates in the 'fast' gated spectra of both samples, while the spectra recorded in 'slow' TG also reveal emission features related to $4f^2 \rightarrow 4f^2$ transitions. In general, the PCL spectra correlate well with the above presented steady-stay XRL spectra. Meanwhile, there are some peculiarities which are worth to be described in more detail.

The $4f^15d^1 \rightarrow 4f^2$ emission band observed in PCL spectrum of 1% Pr^{3+}-doped KLuP extends from about 236 to 380 nm and is composed of two subbands centred at about 272 and 311 nm. The $4f^15d^1 \rightarrow 4f^2$ emission band observed in 5% Pr^{3+}-doped sample is generally shifted towards shorter wavelengths and extends from about 230 to 360 nm while

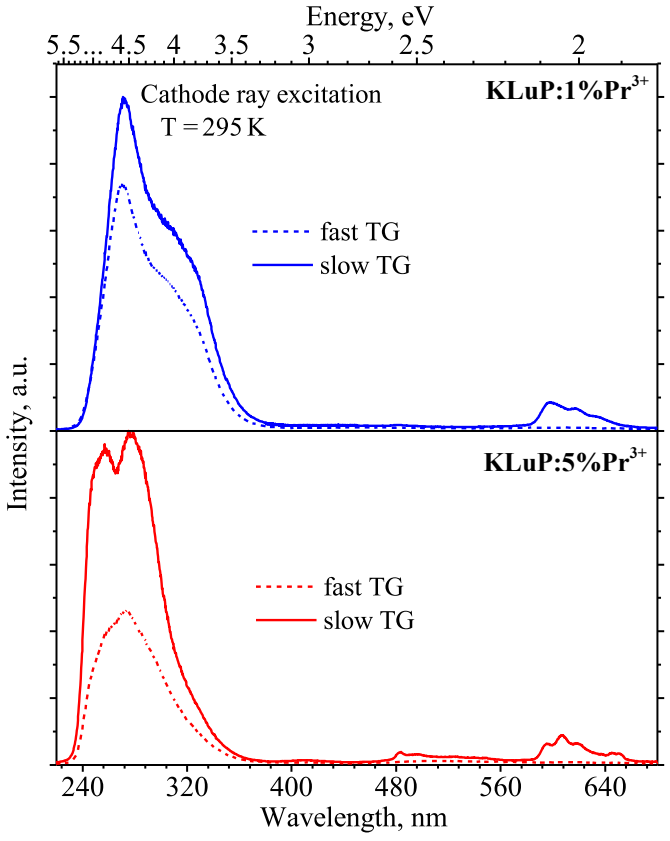

Fig. 3. Time-resolved PCL spectra of $K_3Lu(PO_4)_2$ doped with 1% (top panel) and 5% Pr^{3+} (lower panel) recorded in 'slow' and 'fast' TGs at T = 295 K.

demonstrating two subbands with the well pronounced peaks 256 and 277 nm. Apart from the blue shift, the $4f^15d^1 \rightarrow 4f^2$ emission band of 5% Pr^{3+}-doped sample reveals different band shape in comparison to that observed for the 1%Pr^{3+}-doped sample. Particularly, the shorter wavelength emission sub-band centred near 256 nm is less pronounced that can be explained by self-reabsorption of the high-energy part of the emission arising from high concentration of Pr^{3+} ions. Note that the effect is less significant in the case of X-ray excitation (Fig. 2). We suppose that the observed phenomenon is connected with the variation of spatial distribution of excitation energy within the volume of powdered particles. This, in turn, interfere with the commonly known tendency of lanthanide dopant ions to segregate on surface of particles (nano- and microsize ones) as documented for many inorganic luminescence materials (see Refs. [19–22] and references therein). Simulation of the penetration depth for X- and cathode rays into the KLuP host is presented in Supporting Information (SI). Cathode rays are expected to be absorbed within relatively thin subsurface layer (up to few tens of microns) that results in a higher density of created electronic excitations (and subsequently excited Pr^{3+} ions) near the surface. This is obviously favourable for the self-reabsorption phenomenon demonstrated in the PCL spectra. In turn, X-ray excitation is characterised by higher penetration depth of X-ray photons that leads to greater spatial distribution of electronic excitations within the volume. Self-reabsorption becomes evident for X-ray excitation only at high temperature of 570 K (Fig. 2, lower panel) due to a typical thermal broadening of Pr^{3+} $4f^15d^1 \leftrightarrow 4f^2$ emission and excitation bands.

It is also interesting to note different shape of $4f^15d^1 \rightarrow 4f^2$ emission bands observed in the PCL spectra recorded within 'fast' and 'slow' TGs for the 5%Pr^{3+}-doped sample (see Fig. 3, lower panel). This observation is likely to arise from the presence of delayed recombination processes of host-to-impurity energy transfer that gives rise to time-dependent distribution of electronic excitations within the particles.

We note that the observed phenomena are worth further study that is beyond the scope of the present paper.

4.2. X-ray and cathode-ray excited luminescence decay kinetics

The decay kinetics recorded for $4f^15d^1 \rightarrow 4f^2$ emission in 1% Pr^{3+} and 5% Pr^{3+}-doped KLuP samples upon excitation by single cathode ray pulses and high repetition rate (8 MHz) X-ray synchrotron radiation are presented in Fig. 4. The PCL decay curves of the samples can be well fitted by triple exponential decay function, using the following approximation:

$$I(t) = A_0 + \sum_i A_i . e^{\left(\frac{-t}{\tau_i}\right)} \quad (1)$$

where *Ai* are weighting coefficients for the decay components with lifetimes τ_i (i = 1, 2, 3) while A_0 is a weighting coefficient for the background level. In turn, the XRL decay kinetics virtually depart from exponential behaviour and demonstrate an intense background level resulted from piling-up of slow (microsecond order or longer) decay components excited by continuous sequences of excitation pulses arriving at a high repetition rate as typically observed in synchrotron radiation measurements (see Ref. [23] for details). Meanwhile, the XRL decay can be satisfactory fitted by a double exponential decay function using Eq. (1) (i = 1, 2) and we found the fitting parameters worth presenting for general parametric description of the decay kinetics. The fitting parameters for the PCL and XRL decay curves recorded are gathered in Table 1 while the fitting curves are confronted to the decay curves in Fig. 4.

The PCL decay curves taken for 1% Pr^{3+} and 5% Pr^{3+}-doped samples are dominated by a fast decay component with lifetime (τ_1) of 20.5 and 15.0 ns, respectively. These values are consistent with the Pr^{3+} $4f^15d^1 \rightarrow 4f^2$ emission lifetime documented for some other Pr^{3+}-doped

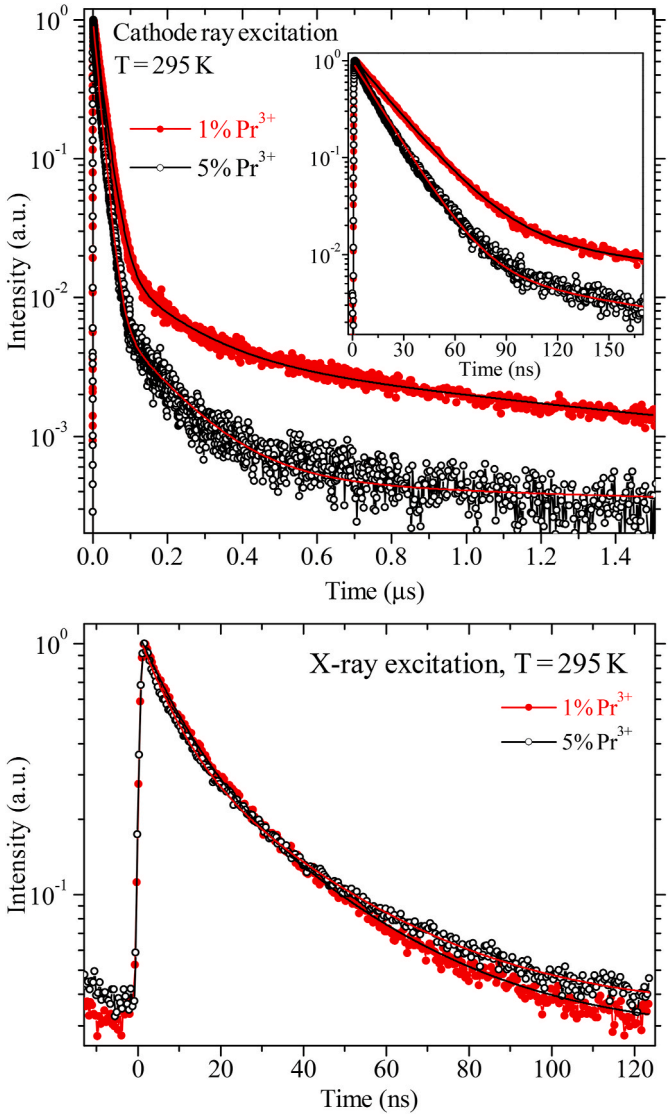

Fig. 4. Luminescence decay kinetics for 1% Pr^{3+} and 5% Pr^{3+}-doped KLuP samples recorded monitoring $4f^15d \rightarrow 4f^2$ emission at 270 nm and 277 nm, respectively, upon excitation by single cathode 120 keV beam pulses (top panel) and high repetition rate X-ray synchrotron radiation (lower panel) at T = 295 K.

Table 1
The fitting parameters for X-ray and cathode ray excited 5 d-4f luminescence decay curves obtained using function (1). Parameter of χ^2 represents goodness of the fitting.

Parameter, unit	Cathode ray excitation		X-ray synchrotron excitation	
	1% Pr^{3+}	5% Pr^{3+}	1% Pr^{3+}	5% Pr^{3+}
τ_1, ns	**20.5**	**15.0**	**6.7**	**4.9**
A_1, a.u.	1.07	0.97	0.57	0.62
τ_2, ns	**148.0**	**130.0**	**24.0**	**23.5**
A_2, a.u.	0.0163	0.009	0.53	0.52
τ_3, ns	**1250.0**	**1140.0**	**-**	**-**
A_3, a.u.	0.0037	0.0025	–	–
A_0, a.u.	3.0×10^{-4}	3.0×10^{-4}	0.028	0.034
χ^2	3.0×10^{-5}	1.1×10^{-4}	4.2×10^{-5}	6.3×10^{-5}

phosphates, viz. $Sr_3La(PO_4)_3$ (17 ns), $Ba_3Lu(PO_4)_3$ (16 ns) and $Ca_9Lu(PO_4)_7$ (17 ns) [24], $KLuP_2O_7$ (20 ns) [13], $LiSrPO_4$ (18 ns) [30], $Sr_9Sc(PO4)7$ (17 ns) [31]. Intensity of the longer PCL decay components with lifetime τ_2 and τ_3 which characterise dynamics of delayed recombination processes are of about two and three orders of magnitude lower, respectively (see Table 1).

It is important to note that the lifetime of the main $4f^15d^1 \rightarrow 4f^2$ emission decay component (20.5 ns) observed for 1% Pr^{3+}-doped KLuP agrees well with earlier reported lifetime of $4f^15d^1 \rightarrow 4f^2$ emission of 1% Pr^{3+}-doped KLuP in RT trigonal phase upon UV intracenter excitation ($\tau \approx$ 20–21 ns) [12, 14]. Meanwhile, the lifetime detected for $4f^15d^1 \rightarrow 4f^2$ emission of 5% Pr^{3+}-doped sample (15 ns) correlates with that observed for low-temperature monoclinic phase ($\tau \approx$ 14.8–15.1 ns) [12, 14]. These observations further indicate that at RT the crystal structure of 1% Pr^{3+}- and 5% Pr^{3+}-doped KLuP samples is of the trigonal and monoclinic phases, respectively.

The decay kinetics recorded upon high repetition rate X-ray excitation demonstrate noticeable contribution of short decay component with lifetime of 6.7 and 4.9 ns for 1% Pr^{3+} and 5% Pr^{3+}-doped samples, respectively, along with longer decay component with lifetime $\tau \sim$24 ns. The presence of the short decay component in the XRL decay curves indicates the non-exponential decay process that can be connected with high repetition rate and high density of excitation that is typical for "white beam" synchrotron excitation [16]. The longer decay component, which intensity and contribution to the yield of decay process is very close to that of the short one, is most probably simultaneously contributed by both normal and delayed decay components of the Pr^{3+} $4f^15d^1 \rightarrow 4f^2$ emission. Unfortunately, getting deeper insight into the relaxation processes observed in the XRL decay kinetics is hardly possible due to the above discussed ambiguity of the exponential fitting model.

4.3. UV photoluminescent spectroscopy

Fig. 5 demonstrates PL (right panel) and PL excitation spectra (left panel) of 1% Pr^{3+} KLuP recorded upon UV excitation at T = 295 K. The emission spectrum obtained upon intracenter $4f^2 \rightarrow 4f^15d^1$ excitation at λ_{exc} = 235 nm (5.29 eV) resembles the above presented RT steady-stay XRL and time-resolved PCL spectra. Visible emission is dominated by broad and relatively weak emission band spread at about 340–560 nm with maximum near 417 nm (2.97 eV) that is excited in the host transparency range at E_{exc} = 4.55 eV (273 nm) and 3.98 eV (312 nm). The same excitation gives rise to weak narrow emission features appeared near 597, 619 and 634 nm and attributed to $^1D_2 \rightarrow {}^3H_4$, $^3P_0 \rightarrow {}^3H_6$, and $^3P_0 \rightarrow {}^3F_2$ intraconfigurational transitions, respectively (see inset in Fig. 5, right panel). An enhancement observed as a tail at the long-wavelength side of the $4f^15d^1 \rightarrow 4f^2$ emission band in region of 320–380 nm indicates contribution of $4f^15d^1 \rightarrow 4f^2$ emission from another Pr^{3+} emission center due to the presence of two crystallographic sites for Pr^{3+} in the RT trigonal phase. The PL excitation spectrum recorded for 1% Pr^{3+} KLuP powder while monitoring $4f^15d^1 \rightarrow 4f^2$ emission band at 313 nm (3.96 eV) is represented by a $4f^2 \rightarrow 4f^15d^1$ excitation band spread from 210 to 256 nm (4.84–5.90 eV) with maximum near 232 nm (5.34 eV) (Fig. 5, left panel). The observed position of $4f^15d^1 \rightarrow 4f^2$ emission band maximum is in very good agreement with the value of 235 nm (5.28 eV) predicted by the Dorenbos model [2, 24] using the data on Ce^{3+} $4f^1 \rightarrow 4f^05d^1$ transition energy in 1% Ce^{3+}-doped KLuP at RT (trigonal phase) [10].

The PL spectrum recorded for 5% Pr^{3+}-doped KLuP upon excitation λ_{exc} = 235 nm (5.29 eV) is dominated by $4f^15d^1 \rightarrow 4f^2$ emission band spread from about 235 to 350 nm (3.54–5.27 eV) without any pronounced enhancement in the range 320–380 nm (Fig. 6, right panel). It is also worth noting that the $4f^2 \rightarrow 4f^2$ emission features are not observed in the PL spectra of 5% Pr^{3+}-doped KLuP. The excitation spectrum recorded for $4f^15d^1 \rightarrow 4f^2$ emission in this sample shows a $4f^2 \rightarrow 4f^15d^1$ excitation band with a maximum near 224 nm (5.54 eV) and a low energy onset near 248 nm (5.0 eV) being generally shifted towards shorter wavelength if compared to similar $4f^2 \rightarrow 4f^15d^1$ excitation band in 1%Pr^{3+}-doped sample.

In general, the shape and position of $4f^15d^1 \rightarrow 4f^2$ and $4f^2 \rightarrow 4f^15d^1$

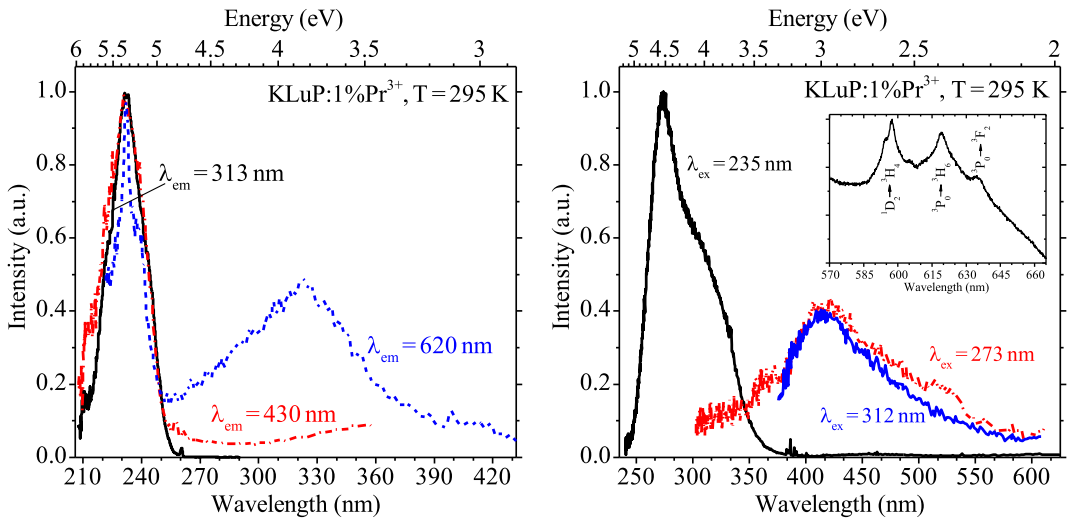

Fig. 5. $K_3Lu(PO_4)_2$:1% Pr^{3+}: PL excitation spectra (left panel) recorded monitoring $4f^2 \rightarrow 4f^2$, $4f^15d^1 \rightarrow 4f^2$ and defect emission and PL spectra recorded upon excitation at $4f^2 \rightarrow 4f^15d^1$ transition and defect excitation band at T = 295 K. Inset in left panel shows fragment of the PL spectrum taken with high resolution using cooled CCD-camera.

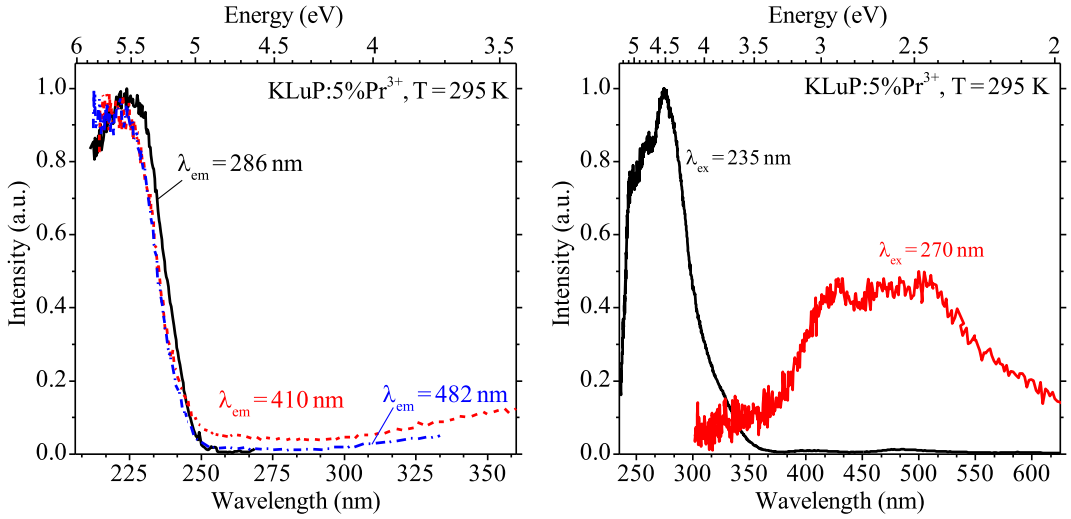

Fig. 6. $K_3Lu(PO_4)_2$:5% Pr^{3+}: PL excitation spectra (left panel) recorded monitoring $4f^15d^1 \rightarrow 4f^2$ and defect emission and PL spectra recorded upon excitation at $4f^2 \rightarrow 4f^15d^1$ transition and defect excitation band at T = 295 K.

bands observed in the PL spectra of 1%Pr^{3+} and 5%Pr^{3+}-doped samples well correspond to those earlier reported for Pr^{3+} in trigonal and monoclinic KLuP, respectively [12,14]. In addition, we note that the PL spectra are in good agreement with the above described results of XRL and PCL measurements (see Figs. 2 and 3).

The Stokes shift for the Pr^{3+} $4f^2 \leftrightarrow 4f^15d^1$ transitions in 1% Pr^{3+}-doped KLuP was estimated in Ref. [14] using deconvolution of the emission and excitation band profiles and resulted to be about 2800 cm^{-1} (~0.35 eV). An estimation of the Stokes shift performed on the basis of PL spectra recorded in this work confirm the value for 1% Pr^{3+}-doped sample while that for 5% Pr^{3+}-doped sample is found to be ~2450 cm^{-1} (~0.30 eV). This observation is worth to be considered within the model for Pr^{3+} emission proposed by Srivastava et al. [28] that suggests $4f^15d^1 \rightarrow 4f^2$ transitions to dominate over $4f^2 \rightarrow 4f^2$ ones when the Stokes shift is lower than 3200 cm^{-1} (~0.4 eV). The statement is well confirmed by the PL spectra of 1% Pr^{3+}-doped sample (Fig. 5, right panel), where $4f^2 \rightarrow 4f^2$ emission lines are just very weak, and further proved by the PL spectra of 5% Pr^{3+}-doped sample where no $4f^2 \rightarrow 4f^2$ emission features are observed.

Another peculiarity of the $4f^2 \rightarrow 4f^2$ emission which should be highlighted here is its dependence on the type of excitation. In particular, emission spectra of KLuP:Pr^{3+} recorded upon excitation with ionising radiation (X-ray or cathode ray) demonstrate more pronounced $4f^2 \rightarrow 4f^2$ emission features in the spectral range of 580–630 nm (Figs. 2 and 3) than those recorded upon selective intracentre excitation at $4f^2 \rightarrow 4f^15d^1$ absorption band (Fig. 5). Such a behaviour suggests that the host lattice defects that capture intrinsic host electronic excitations of the host are capable to transfer energy to the Pr^{3+} ^3P_J and $^1D_2$ energy levels that is obviously promoted by the spectral overlap. We also note that in case of 1% Pr^{3+}-doped KLuP sample the excitation spectra recorded for emission detected at 430 nm (due to defects) and 620 nm (defect plus $4f^2 \rightarrow 4f^2$ emission) demonstrate well pronounced excitation band in the range of $4f^2 \rightarrow 4f^15d^1$ transitions. This indicates the presence of energy transfer from the Pr^{3+} $4f^15d^1$ state to the defects. It is also worth mentioning that the collected emission spectra do not reveal any $4f \rightarrow 4f$ emission lines with energy exceeding that for $^3P_0 \rightarrow {}^3H_4$ as $^1S_0$ state (~5.77 eV) is located above the lowest $4f^15d^1$ mixed-states [2].

Thus, we conclude that the materials studied here demonstrate defect-related emission which spectral appearance and emission intensity depend on the phase composition of the host. The defects form

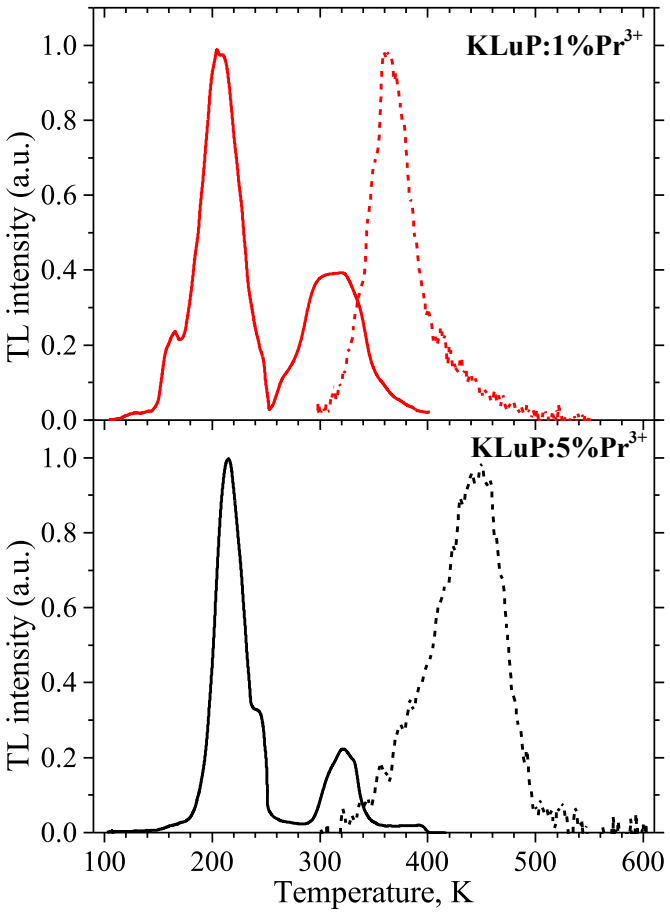

Fig. 7. Normalized TL curves recorded monitoring $4f^15d \rightarrow 4f^2$ emission at 278 nm for 1% Pr^{3+}- (top panel) and 5% Pr^{3+}-doped KLuP (bottom panel) after X-ray irradiation at T = 90 K (solid lines) and 295 K (dashed lines).

competitive paths for capture and relaxation of electronic excitations that obviously limit the efficiency of recombinational mechanism of host-to-impurity energy transfer.

4.4. Thermoluminescent measurements

Delayed recombination emission processes are often considered to be connected with retrapping of electrons and/or holes by host defects (see e.g. Ref. [4] and references therein). In order to evaluate the energy structure and density of defects in this material we studied TL glow curves while monitoring Pr^{3+} $4f^15d^1 \rightarrow 4f^2$ emission (Fig. 7). After X-ray irradiation at T = 90 K the $4f^15d^1 \rightarrow 4f^2$ emission in the samples is well triggered by thermal stimulation while demonstrating a complex structure of thermoluminescence (TL). The most pronounced glow peaks are observed in the regions of 204–214 K and 312–322 K for 1% Pr^{3+}- and 5% Pr^{3+}-doped KLuP samples, respectively, being generally shifted towards higher temperature for the 5% Pr^{3+}-doped sample (Fig. 7, solid lines). After X-ray irradiation at RT, the TL curves are dominated by broad non-uniform peaks with maxima at 362 K and 442 K for 1% Pr^{3+}- and 5% Pr^{3+} - doped KLuP samples, respectively (Fig. 7, dashed lines).

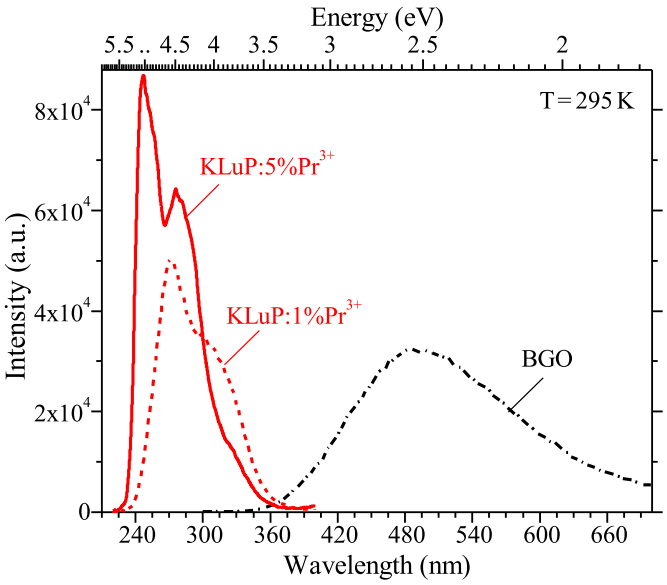

Fig. 8. The comparison of XRL spectra of 1% Pr^{3+}- and 5% Pr^{3+}-doped KLuP and BGO powders recorded in identical conditions, T = 295 K.

These observations indicate the presence of several trapping centers with different activation energy. The temperature dependences of XRL output monitored for $4f^15d \rightarrow 4f^2$ emission (see Inset in Fig. 2) demonstrate gradual rise of XRL output while temperature increases up to about 300–400 K, i.e. well above the carriers delocalization temperature as determined from the TL glow curves measurements (Fig. 7, solid lines). We note that none of the TL peaks can be straightforward related to phase transition processes. As an example it is worth considering the 1%Pr^{3+}-doped KLuP sample that is expected to have monoclinic to trigonal phase transition at about 250 K while it demonstrates the most pronounced TL peak at noticeably lower temperature of 206 K.

We further note that the TL peaks, maximum of the XRL temperature dependence, and XRL quenching temperature T_Q observed for the 5% Pr^{3+}-doped KLuP are all systematically shifted towards higher temperature relative to those observed for the 1% Pr^{3+}-doped KLuP. Like the above spectroscopic data, these facts point to different local environment of the impurity Pr^{3+} ion in 1% Pr^{3+}- and 5% Pr^{3+}-doped KLuP that is related to different phase composition.

The TL glow curves were approximated using a function based on the analytical equation proposed by Kitis et al. [29] for a TL peak of general-order kinetics. The method allows the calculation of parameters for every peak in a TL curve containing multiple glow peaks using the following analytic expressions:

$$I(T) = I_m b^{b/(b-1)} \exp\left(\frac{E}{kT}\frac{T-T_m}{T_m}\right).\left[(b-1)(1-\Delta)\frac{T^2}{T_m^2}\exp\left(\frac{E}{kT}\frac{T-T_m}{T_m}\right)+Z_m\right]^{-b/(b-1)} \quad (2)$$

$$s = \frac{\beta E}{kT_m^2}\frac{1}{Z_m}\exp\left(\frac{E}{kT_m}\right) \quad (3)$$

where, $I(T)$ is TL intensity with maximum of I_m, b is kinetics order, E – energy trap depth, T_m is temperature at the peak maximum, $\Delta = 2\,kT/E$, $\Delta_m = 2kT_m/E$, $Z_m = 1 + (b-1)\Delta_m$. In equation (3), s stands for a frequency factor, β is a heating rate. Each peak is fitted by separate fitting function. By summarizing the obtained approximation curves once can

Table 2
The calculated TL parameters from the deconvolution of the experimental TL curves.

Composition	Calculated parameters			
	TL peak, K	E (eV)	b	s (s^{-1})
KLuP:1% Pr^{3+}	206	0.33	2	$1{\cdot}10^{8}$
	311	0.46	2	$3{\cdot}10^{7}$
	363	0.83	2	$8{\cdot}10^{9}$
KLuP:5% Pr^{3+}	215 K	0.46	2	$2{\cdot}10^{9}$
	321 K	0.92	2	$1{\cdot}10^{13}$
	443 K	0.52	1	$5{\cdot}10^{6}$

reproduce the original TL glow curve. The TL parameters calculated using equations (2) and (3) are presented in Table 2. Meanwhile, an important conclusion that comes out of the TL results is a clear indication of the presence of defects (carrier capture centres) in the materials, which certainly contribute into Pr^{3+} recombination luminescence output.

4.5. Light output

Among the most important characteristics of scintillator materials is their light output (LO). An absolute LO is typically measured and compared through studying of amplitude spectra upon gamma-ray excitation [25, 26]. The approach is well suitable for bulk crystals and provides best accuracy when the sample under study and a standard (reference) sample have similar emission spectra. Since, we deal with a microcrystalline powder, the approach can hardly be applied. Moreover, emission of a commercial $Bi_4Ge_3O_{12}$ (BGO) used as a reference sample appears at spectral range different to that of KLuP:Pr^{3+} and is characterised by a much longer decay time (~300 ns). These issues prevent from correct measurement and comparison of the corresponding amplitude spectra. In this connection, we found it most reasonable to estimate a relative LO upon X-ray excitation.

To perform the study, a commercial $Bi_4Ge_3O_{12}$ (BGO) single crystal was ground to powder in an agate mortar. The XRL spectra of 1% Pr^{3+}- and 5% Pr^{3+}-doped KLuP and BGO samples recorded in the identical conditions are shown in Fig. 7. We note that the 5% Pr^{3+}-doped sample provides noticeably higher LO relative to the 1%Pr^{3+}-doped one. It is interesting to compare this observation with the opposite one documented for Pr-doped $YAlO_3$ [32]. We suppose that in the case of KLuP:Pr^{3+}, the increase of Pr^{3+} concentration makes recombination on Pr^{3+} sites more favourable within their competition with the defects (and quenching sites) while high (5%) concentration of Pr^{3+} in $YAlO_3$ represent an onset of typical concetration quenching.

To quantitively compare the LO, the total area of the KLuP:Pr^{3+} XRL spectra were integrated in the range of 230–390 nm (Pr^{3+} $4f^15d^1{\rightarrow}4f^2$ emission) and for BGO in the range of 350–700 nm (emission due to self-trapped excitons [27]). The integral LO of 1% Pr^{3+}- and 5% Pr^{3+}-doped KLuP samples was found to be about 110% and 160% of that for BGO, respectively. We remind that the absolute LO of the latter is about 8500 photons/MeV [26]. It is worth noting that Wisniewski et al. [11] determined an absolute LO of 1% Ce^{3+}-doped KLuP (26500 photons/MeV) that is similar to LO of the best figure-of-merit scintillators. All these facts suggest that KLuP:Pr^{3+} is potentially suitable for scintillator application. Our observations also suggest that higher Pr^{3+} content is favourable for obtaining the high LO. We believe that increase of the LO is mostly related to Pr^{3+} content rather than due to phase transition issues of the host. The latter is supported by the results presented in Ref. [14] where LO of Pr^{3+} $4f^15d{\rightarrow}4f^2$ emission in $K_3Lu_{1-x}Y_x(PO_4)_2$:1% Pr^{3+} is shown to be nearly independent of Y^{3+} content.

5. Conclusions

In summary, KLuP doped with 1% and 5% Pr^{3+} ions have been synthesized by a solid state reaction and analysed by XRD technique. The temperature-dependent luminescence spectroscopic characterisation performed upon X-, cathode ray and UV excitation allowed to demonstrate that at RT 1% Pr^{3+}-doped KLuP contains single trigonal phase, while the 5% Pr^{3+}-doped KLuP keeps monoclinic phase and turns to trigonal phase well above RT. In other words, a high concentration of Pr^{3+} ions in KLuP:Pr^{3+} increases the stability of the KLuP monoclinic phase so that luminescence spectroscopic and decay kinetics characteristics representing evidence of phase transition occur at much higher temperature than in case of moderate doping level. This is the first observation of a high-temperature phase transition taking place in KLuP:Pr^{3+}.

Upon both direct intra-center and band-gap excitation the emission is dominated by Pr^{3+} high intensity interconfigurational $4f^15d{\rightarrow}4f^2$ radiative transitions while of $4f^2{\rightarrow}4f^2$ intraconfigurational transitions is weakly pronounced because of the small Stokes shift revealed for the $4f^15d{\leftrightarrow}4f^2$ transitions.

The Pr^{3+} $4f^15d{\rightarrow}4f^2$ emission in KLuP:Pr^{3+} excited by X-ray synchrotron or pulsed cathode beams demonstrate complex decay kinetics which tend become accelerated for the sample with higher Pr^{3+} concentration. The latter is accompanied by a blue shift of the Pr^{3+} $4f^15d{\rightarrow}4f^2$ emission and decrease of Stokes shift and is determined by the phase changes resulting in increase of the covalency of the Pr–O bonds. The XRL and PCL decay kinetics also reveal the presence of longer decay components (of sub-microsecond and longer lifetime) which are best observed in the PCL decay curves measurements. Appearance of the longer decay components representing delayed recombination of charge carriers on Pr^{3+} $4f^15d$ states is shown to be connected with the presence defects (as demonstrated by TL measurements) which form competitive channels for relaxation and re-trapping of intrinsic electronic excitation. For this reason, a higher concentration of Pr^{3+} dopant ions is more favourable for efficient host-to-impurity energy transfer. The latter is well demonstrated by the study of integrated LO upon X-ray excitation that was found to be 110% and 160% of that for standard BGO for 1% Pr^{3+}- and 5% Pr^{3+}-doped KLuP samples, respectively.

Declaration of competing interest

The authors declare that they have no known competing financial interests or personal relationships that could have appeared to influence the work reported in this paper.

Acknowledgments

The work was partially supported by the Ministry of Science and Higher Education of the Russian Federation (through the basic part of the government mandate, project No. FEUZ-2020-0060), Act 211 Government of the Russian Federation (contract N° 02.A03.21.0006), STSM grant from COST Action TD1401 ″FAST" as well as by Estonian Research Council (project PRG629) and Estonian Center of Excellence in Research "Advanced materials and high-technology devices for sustainable energetics, sensorics and nanoelectronics" TK141 (project No. 2014-2020.4.01.15-0011) by the ERDF funding in Estonia. The time-resolved X-ray excited measurements were performed at the Shared research center SSTRC based on the NovoFEL/VEPP-4 - VEPP-2000 facilities at Budker Institute of Nuclear Physics (Siberian Branch of Russian Academy of Sciences, Novosibirsk, Russia) while using experimental equipment funded by RFMEFI62119X0022 project. Authors thank Erica Viviani (University of Verona) for assistance in the synthesis of the samples and Yulya Khatchenko (UrFU, Ekaterinburg) for assistance in the processing the experimental data. F. P. and M. B. thank the Facility "Centro Piattaforme Tecnologiche" of the University of Verona for access to the Thermo ARL X'TRA powder diffractometer.

Appendix A. Supplementary data

Supplementary data to this article can be found online at https://doi.org/10.1016/j.jlumin.2020.117749.

CRediT author statement

Konstantin V. Ivanovskikh: Conceptualization, Validation, Methodology, Data curation, Writing-Original draft, Reviewing and Editing. **Vladimir A. Pustovarov**: Conceptualization, Methodology, Investigation, Writing-Original draft, Reviewing and Editing, Funding acquisition. **Sergey Omelkov:** Data acquisition, Data curation, Writing and Editing. **Marco Kirm:** Methodology, Investigation, Reviewing and Editing. **Fabio Piccinelli:** Validation, Methodology, Data curation, Editing. **Marco Bettinelli:** Conceptualization, Methodology, Reviewing and Editing, Supervision.

References

[1] M. Nikl, H. Ogino, A. Yoshikawa, E. Mihokova, J. Pejchal, A. Beitlerova, A. Novoselov, T. Fukuda, Fast 5*d*-4*f* luminescence of Pr^{3+} in Lu_2SiO_5 single crystal host, Chem. Phys. Lett. 410 (2005) 218, https://doi.org/10.1016/j.cplett.2005.04.115.

[2] A.M. Srivastava, Aspects of Pr^{3+} luminescence in solids, J. Lumin. 169 (2016) 445, https://doi.org/10.1016/j.jlumin.2015.07.001.

[3] A. Zych, M. de Lange, C.d.M. Donega, A. Meijerink, Analysis of the radiative lifetime of Pr^{3+} *d-f* emission, J. Appl. Phys. 112 (2012), 013536, https://doi.org/10.1063/1.4731735.

[4] M. Nikl, V.V. Laguta, A. Vedda, Complex oxide scintillators: material defects and scintillation performance, Phys. Status Solidi 245 (2008) 1701–1722, https://doi.org/10.1002/pssb.200844039.

[5] J.M. Ogiegło, A. Zych, K.V. Ivanovskikh, T. Jüstel, C.R. Ronda, A. Meijerink, Luminescence and energy transfer in $Lu_3Al_5O_{12}$ scintillators co-doped with Ce^{3+} and Tb^{3+}, J. Phys. Chem. C 116 (2012) 8464–8474, https://doi.org/10.1021/jp301337f.

[6] M. Conti, L. Eriksson, H. Rothfuss, C.L. Melcher, Comparison of fast scintillators with TOF PET potential, IEEE Trans. Nucl. Sci. 56 (2009) 926–933, https://doi.org/10.1109/TNS.2008.2009446.

[7] K.V. Ivanovskikh, A. Meijerink, F. Piccinelli, A. Speghini, E.I. Zinin, C. Ronda, M. Bettinelli, Optical spectroscopy of $Ca_3Sc_2Si_3O_{12}$, $Ca_3Y_2Si_3O_{12}$ and $Ca_3Lu_2Si_3O_{12}$ doped with Pr^{3+}, J. Lumin. 130 (2010) 893–901, https://doi.org/10.1016/j.jlumin.2009.12.031.

[8] A.J. Wojtowicz, W. Drozdowski, D. Wisniewski, J.-L. Lefaucheur, Z. Galazka, Z. Gou, T. Lukasiewicz, J. Kisielewski, Scintillation properties of selected oxide monocrystals activated with Ce and Pr, Opt. Mater. 28 (2006) 85–93, https://doi.org/10.1016/j.optmat.2004.09.029.

[9] K.V. Ivanovskikh, Q. Shi, M. Bettinelli, V.A. Pustovarov, Unraveling Pr^{3+} 5*d*-4*f* emission in $LiLa_9(SiO_4)_6O_2$ crystals doped with Pr^{3+} ions, Opt. Mater. 79 (2018) 108, https://doi.org/10.1016/j.optmat.2018.03.006.

[10] V.A. Pustovarov, A.N. Razumov, D.I. Vyprintsev, Luminescence of $LaBr_3$:Ce,Hf crystals under photon excitation in the ultraviolet, vacuum ultraviolet, and X-ray ranges, Phys. Solid State 56 (2014) 347, https://doi.org/10.1134/S1063783414020267.

[11] D. Wisniewski, A.J. Wojtowicz, W. Drozdowski, J.M. Farmer, L.A. Boatner, Scintillation and luminescence properties of Ce-activated $K_3Lu(PO_4)_2$, J. Alloys Compd. 380 (2004) 191, https://doi.org/10.1016/j.jallcom.2004.03.042.

[12] M. Trevisani, K.V. Ivanovskikh, F. Piccinelli, M. Bettinelli, Fast 5*d*-4*f* luminescence in Pr^{3+}-doped $K_3Lu(PO_4)_2$, J. Lumin. 152 (2014) 2–6, https://doi.org/10.1016/j.jlumin.2013.11.068.

[13] M. Trevisani, K. Ivanovskikh, F. Piccinelli, M. Bettinelli, Synchrotron radiation study of interconfigurational 5*d*-4*f* luminescence of Pr^{3+} in $KLuP_2O_7$, Z. Naturforsch. B Chem. Sci. 69b (2014) 205, https://doi.org/10.5560/znb.2014-3260.

[14] I. Carrasco, K. Bartosiewicz, F. Piccinelli, M. Nikl, M. Bettinelli, Structural effects and 5*d*-4*f* emission transition shifts induced by Y co-doping in Pr-doped $K_3Lu_{1-x}Y_x(PO_4)_2$, J. Lumin. 189 (2017) 113–119, https://doi.org/10.1016/j.jlumin.2016.08.022.

[15] J.M. Farmer, L.A. Boatner, B.C. Chakoumakos, C.J. Rawn, D. Mandrus, R. Jin, J. C. Bryan, Polymorphism, phase transitions, and thermal expansion of $K_3Lu(PO_4)_2$, J. Alloys Compd. 588 (2014) 182–189, https://doi.org/10.1016/j.jallcom.2013.10.232.

[16] V.A. Pustovarov, E.I. Zinin, A.L. Krymov, B.V. Shulgin, Some peculiarities of the luminescence of inorganic scintillators under excitation by high intensity synchrotron radiation, Rev. Sci. Instrum. 63 (1992) 3521, https://doi.org/10.1063/1.1143760.

[17] S.I. Omelkov, V. Nagirnyi, E. Feldbach, R.M. Turtos, E. Auffray, M. Kirm, P. Lecoq, Intraband luminescence excited in new ways: low-power x-ray and electron beams, J. Lumin. 191 (2017) 61–67, https://doi.org/10.1016/j.jlumin.2017.02.001.

[18] R.D. Shannon, Revised effective ionic radii and systematic studies of interatomic distances in halides and chalcogenides, Acta Crystallogr. A 32 (1976) 751–767, https://doi.org/10.1107/S0567739476001551.

[19] B. Cojocaru, D. Avram, V. Kessler, V. Parvulescu, G. Seisenbaeva, C. Tiseanu, Nanoscale insights into doping behavior, particle size and surface effects in trivalent metal doped SnO_2, Sci. Rep. 7 (2017) 9598.

[20] D. Yuan, G. Shun Yi, G.M. Chow, Effects of size and surface on luminescence properties of submicron upconversion $NaYF_4$:Yb,Er particles, J. Mater. Res. 24 (2011) 2042–2050.

[21] S.-J. Shih, Y.-Y. Wu, K.B. Borisenko, Control of morphology and dopant distribution in yttrium-doped ceria nanoparticles, J. Nanoparticle Res. 13 (2011) 7021–7028.

[22] R.K. Sharma, Y.N. Chouryal, A.I. Slesarev, K.V. Ivanovskikh, I.I. Leonidov, S. Nigam, P. Ghosh, A closer look at the defects and luminescence of nanocrystalline fluorides synthesized via ionic liquids: the case of Ce^{3+}-doped BaF_2, New J. Chem. 44 (2020) 200–209.

[23] D. Wisniewski, L.A. Boatner, Scintillation properties and time-resolved spectroscopy of a novel scintillator material: Ce^{3+}-activated $Li_3Lu(PO_4)_2$ crystals, IEEE Trans. Nucl. Sci. 56 (2009) 3806–3818, https://doi.org/10.1109/TNS.2009.2032290.

[24] M. Trevisani, K.V. Ivanovskikh, F. Piccinelli, A. Speghini, M. Bettinelli, Interconfigurational 5*d*→4*f* luminescence of Ce^{3+} and Pr^{3+} in $Ca_9Lu(PO_4)_7$, J. Phys. Condens. Matter 24 (2012), 385502, https://doi.org/10.1088/0953-8984/24/38/385502.

[25] C.L. Melcher, R.A. Manente, J.S. Schweitzer, Applicability of barium fluoride and cadmium tungstate scintillators for well logging, IEEE Trans. Nucl. Sci. 36 (1989) 1188–1192, https://doi.org/10.1109/23.34629.

[26] M. Moszynski, M. Kapusta, M. Mayhugh, D. Wolski, S.O. Flyckt, Absolute light output of scintillators, IEEE Trans. Nucl. Sci. 44 (1997) 1052–1061, https://doi.org/10.1109/23.603803.

[27] V.Yu Ivanov, A.V. Kruzhalov, V.A. Pustovarov, V.L. Petrov, Electron excitation and luminescence in $Bi_4Ge_3O_{12}$ and $Bi_4Si_3O_{12}$ crystals, Nucl. Instrum. Methods Phys. Res. A 261 (1–2) (1987) 150–152, https://doi.org/10.1016/0168-9002(87)90585-7.

[28] A.M. Srivastava, M. Jennings, J. Collins, The interconfigurational ($4f^15d^1 \rightarrow 4f^2$) of Pr^{3+} luminescence in $LuPO_4$, $K_3Lu(PO_4)_2$ and $LiLuSiO_4$, Opt. Mater. 34 (2012) 1347, https://doi.org/10.1016/j.optmat.2012.02.016.

[29] G. Kitis, J.M. Gomez-Ros, J.W.N. Tuyn, Thermoluminescence glow-curve deconvolution functions for first, second and general orders of kinetics, J. Phys. D Appl. Phys. 31 (1998) 2636–2641, https://doi.org/10.1088/0022-3727/31/19/037.

[30] V.A. Pustovarov, K.V. Ivanovskikh, Yu E. Khatchenko, Q. Shi, M. Bettinelli, Energy conversion in $LiSrPO_4$ doped with Pr^{3+} ions, Radiat. Meas. 123 (2019) 39–43, https://doi.org/10.1016/j.radmeas.2019.01.016.

[31] V.A. Pustovarov, K.V. Ivanovskikh, YuE. Khatchenko, V.Yu Ivanov, M. Bettinelli, Q. Shi, Luminescence of Pr^{3+} impurity centers and defects in $Sr_9Sc(PO4)7:Pr^{3+}$, Phys. Solid State 61 (5) (2019) 758–762, https://doi.org/10.1134/S1063783419050275.

[32] M. Zhuravleva, A. Novoselov, A. Yoshikawa, J. Pejchal, M. Nikl, T. Fukuda, Crystal growth and scintillation properties of Pr-doped YAlO3, Opt. Mater. 30 (2007) 171–173, https://doi.org/10.1016/j.optmat.2006.11.057.